VERTICAL FLUX OF TRACER IN THE GULF OF MEXICO: THE IMPACT OF SMALL SCALE DYNAMICS AND STORMS

Jouanno[1], J., X. Capet[2], J. Sheinbaum[3], F. Durand[1], R. Dussurget[4], and E. P. Chassignet[5]

1 LEGOS, Université de Toulouse, IRD, CNRS, CNES, UPS, Toulouse, France.

2 CNRS-IRD-Sorbonne Universités, UPMC, MNHN, LOCEAN Laboratory, Paris, France

3 Departamento de Oceanografía Física, CICESE, Ensenada, Baja California, Mexico

4 Mercator Ocean, Ramonville-Saint-Agne

5 Center for Ocean-Atmospheric Prediction Studies, Florida State University, Tallahassee, FL, USA

Corresponding author: Julien Jouanno (julien.jouanno@ird.fr)

Key Points:

- High resolution simulations of the Gulf of Mexico have been developed
- Eddy activity on scales shorter than the mesoscale reduces the exchanges between the surface and the thermocline
- Restratifying action of the submesoscale turbulence limits the deepening of the mixed-layer

Abstract

In a series of regional simulations (with horizontal resolution at ¼°, 1/12° and 1/36°), configured to investigate the role played by the meso- and submesoscale turbulence on the dispersion of passive tracers in the upper layers of the Gulf of Mexico, we show that eddy activity on scales shorter than the mesoscale reduces the exchanges between the surface and the thermocline. This is in contrast to previous studies which suggest that enhanced submesoscale activity in the winter mixed layer may actually lead to increased exchanges with the permanent thermocline. This reduction is explained by the restratifying action of the submesoscale turbulence that effectively limits the deepening of the mixed-layer in response to atmospheric winter synoptic events.

1. Introduction

Submesoscale processes, including eddies and filaments at scale of O (10) km and below, have received increasing attention in recent years, stimulated by their potential key role in the energy dissipation of the balanced flows (Capet et al. 2008, Capet et al. 2016), their impact on the large scale circulation (Lévy et al. 2010) or their consequences on the biogeochemistry (Mahadevan and Archer 2000, Lévy et al. 2001, Lévy et al. 2012). Submesoscale oceanic currents have multiple origins, the most predominant being mixed-layer instability, strain induced frontogenesis or topographic wake (see the review by McWilliams 2016).

Despite a growing understanding of the processes involved in their generation and their recognized importance on the ocean functioning, the overall impact of the submesoscale dynamics on the vertical tracer fluxes remains ambiguous. It involves competing effects whose balance is likely to be region dependent. On the one hand, the prevailing paradigm is that, at submesoscale, the breakdown of the geostrophic balance leads to large vertical velocities that increase the vertical exchanges between the mixed-layer and the ocean below (e.g. Klein and Lapeyre, 2009, Zhong and Bracco 2013, Rosso et al. 2014). On the other hand, the submesoscale eddy tracer fluxes also act to vertically restratify the upper ocean, limiting the deepening of the mixed-layer under surface cooling conditions and speeding up the restratification (Fox-Kemper et al. 2008, Capet et al. 2008, Couvelard et al. 2015). Such control on the mixed-layer depth may in turn limit the vertical tracer exchanges between the subsurface and the mixed-layer. Observations cannot settle this issue but some studies have recently downplayed the role of submesoscale vertical tracer fluxes between the interior ocean and the near-surface (e.g., Ascani et al. 2013).

The ubiquity and seasonal variability of small-scale eddies and filaments in the Gulf of Mexico (GoM) is illustrated by the winter and summer surface vorticity snapshots displayed in Figure 1. Despite its potential importance in driving tracers or pollutant dispersion, air-sea exchanges and the biogeochemistry of the region, the interest in submesoscale eddy activity in the GoM is quite recent and mainly focused on the northern part of the basin (Zhong and Bracco 2013, Luo et al. 2016, Bracco et al. 2016). Comparing two simulations of the GoM at 5 and 1 km horizontal resolution, Zhong and Bracco (2013) found that vertical dispersion of neutrally buoyant water parcels increases when increasing the resolution. More recently, Luo et al. (2016) evidenced from a high resolution model (1.6 km horizontal resolution) two seasonal peaks of submesoscale activity in the northern GoM: a winter peak associated with deep mixed-layers and large available potential energy and a summer peak due to the intense lateral density gradients created by the Mississippi plume (see also Hetland 2017).

The main focus of this study is to clarify the role played by the mesoscale and submesoscale turbulence in controlling the exchanges between the surface and the subsurface of the GoM. Three regional simulations, including a passive tracer sub-model, were performed over a range of horizontal resolution (1/4°, 1/12°, 1/36°) covering eddy present to submesoscale-rich regimes for a period of 20 years. The model experiments are described in Section 2. The mean and seasonal distribution of the meso- to submesoscale activity in the GoM are described from along-track altimetry and our highest resolution simulation (1/36°) in Section 3. The impact of the submesoscale activity on the vertical fluxes of a passive tracer initialized with a vertical profile typical of winter nutrient distribution is presented and discussed in Section 4. The results are summarized and discussed in Section 5.

2. Model and simulations description

The numerical code is the oceanic component of the Nucleus for European Modeling of the Ocean program (NEMO3.6, Madec, 2016). It solves the three dimensional primitive equations in spherical coordinates discretized on a C-grid and fixed vertical levels (z-coordinate). Temperature and salinity are advected using a Total Variance Dissipation scheme (TVD) with nearly horizontal diffusion parameterized as a Laplacian isopycnal diffusion. The horizontal diffusion of momentum is implicit by using the third order upstream advection scheme UP3. The vertical diffusion coefficients are given by a Generic Length Scale (GLS) scheme with a k-ε turbulent closure (Umlauf and Burchard 2003, Reffray et al. 2015). Bottom friction is quadratic with a bottom drag coefficient of 10^{-3} and free slip boundary conditions are applied at the lateral boundaries. The temporal integration is carried out with a modified Leap Frog Asselin Filter (Leclair and Madec 2009), with a coefficient of 0.1. The free-surface is solved using a time-splitting technique with the barotropic part of the dynamical equations integrated explicitly with 60 sub time-steps of the baroclinic time step.

The model is forced at its lateral boundaries with daily outputs from the MERCATOR global reanalysis GLORYS2V3. The open boundary conditions radiate perturbations out of the domain and relax the model variables to 1-day averages of the reanalysis data. Details of the method are given in Madec (2016). At the surface, the atmospheric fluxes of momentum, heat and freshwater are computed by bulk formulae (Large and Yeager, 2009). The model is forced with DFS5.2 product (Dussin et al. 2016) which is based on ERA-Interim reanalysis and consists of 3-hour fields of wind, atmospheric temperature and humidity, and daily fields of long, short wave radiation and precipitation. The shortwave radiation forcing is modulated by a theoretical diurnal cycle. A monthly climatological runoff based on the data set of Dai and Trenberth (2002) is prescribed near the river mouths as a surface freshwater flux with increased vertical mixing in the upper 10 meters.

The regional model configuration consists of a domain encompassing the GoM and the Cayman Sea (from 98°W to 78°W and from 14°N to 31°N), with 75 levels in the vertical (with 12 levels in the upper 20 meters and 24 levels in the upper 100 meters). Three numerical experiments at ¼°, 1/12° and 1/36° horizontal resolution have been conducted. Their main characteristics and differences are summarized in Table 1. The three simulations have been integrated from 1 January 1993 to 31 December 2012. They have been initialized using geostrophic balance and the temperature and salinity fields obtained from ¼° outputs of MERCATOR GLORYS2V3 reanalysis at day 1 January 1993. The 1/36° configuration has been used in Jouanno et al. (2016a) to study the formation of short-period Loop Current Frontal Eddies (LCFEs). We refer the reader to this publication for a validation of the background state (currents and eddy kinetic energy; EKE) and a detailed comparison of the model LCFEs with in-situ and satellite observations.

In order to quantify the impact of the high frequency winds on the vertical exchanges of tracers, three parallel simulations at 1/4°, 1/12° and 1/36° were carried out with monthly wind stress. In this set of simulations (which will be referred as MONTHLY) the surface wind stress is computed using monthly averages of the 3-hourly DFS5.2 winds used in the reference simulations. Note that in order to identify the role of the mechanical contribution of the high frequency winds (and not their direct impact on the air-sea fluxes), the air–sea heat and freshwater fluxes (specifically the latent and sensible heat fluxes and the evaporation) in MONTHLY simulations are computed using the high-frequency DFS5.2 winds just like in the reference simulations.

The simulations also include a passive tracer $TR_{nutrient}$ freely transported by the flow and entrained by vertical mixing. The passive tracers are advected and diffused with the same scheme employed with the active tracers (see above). Following the strategy of Levy et al. (2012), the tracer is initially uniformly distributed in the horizontal and, as real nutrients do, increases with depth from 0 at the surface to 1 at 200 m depth and beyond (i.e. below the euphotic depth) in a hyperbolic tangent manner. The tracer is initialized at days Jan 1, Mar 15, May 27, Aug 8, and Oct 20 of each year and integrated each time for a period of 73 days. This sums to a total of 100 realizations for the period 1993-2012. The connection between the dynamics of this passive tracer and that of nutrients in the real ocean is discussed in the conclusions.

3. Meso- and submesoscale surface energy distribution in the Gulf of Mexico: comparison between model and along track altimetry

3.1 Along track sea level data

In order to asses the realism of the meso and submesoscale field resolved by the high resolution GOLFO36 model, we compared surface properties with two different along-track altimeters: Jason2 (for the period 2009-2012) and Saral/Altika (period 2013-2015). We choose these altimeters because of their complete coverage of the area of interest, their performance and their low noise level in the submesoscale range (e.g. Dufau et al. 2016). As in Le Hénaff et al. (2014) we use 1Hz delayed time level-3 sea surface height data not filtered, nor sub-sampled. Jason2 has a repeat period of 10 days for each track, while Altika has a repeat period of 35 days. We computed spectra of both altimetric datasets as follows. Tracks with gaps larger than 18km were removed. The spatial coverage is optimized by segmenting the along track signal into slices of ~600 km (as in Dufau et al. 2016) with 50% of authorized overlap between slices. One consequence is that the offshore areas have more weight in the averaged spectra than coastal areas. The model data are interpolated along the tracks with repeat periods similar to the observations.

The wavenumber sea level spectra from Jason2 and Altika exhibit spectral slopes close to k^{-4} (Figure 2a). This slope is consistent with global analysis of Xu and Fu (2012) who found a slope close to k^{-4} in the subtropical areas. At wavelengths below 100 km, the model spectral slope is steeper than the altimetry slope. In this range, uncertainties are large and there are many possible sources of discrepancy between model and altimeter spectra: i) instrumental noise that increase the level of energy seen in altimetry at short scales (particularly so for Jason2, which shows significantly more energy than AltiKA there), ii) the sea surface signature of internal tides that are not represented in our model configuration and presumably have a significant effect on sea level fine-scale variability (Shriver et al. 2012), iii) the use of model daily averages which smooth the sea level gradients, and iv) limited effective resolution of our 1/36° grid. At wavelengths between 600 km and 100 km, the model sea level spectral slope is in very good agreement with the satellite observations, suggesting that the model adequately represents KE transfers across scale in this wavelength range.

3.2 Kinetic energy

Along-track kinetic energy has been computed using i) geostrophic velocities obtained from altimetry sea level (Figures 3a,b) ii) geostrophic velocities obtained from model (GOLFO36) sea level (Figures 3c,d), and iii) model (GOLFO36) surface velocities normal to the track (Figures 3e,f). The sea level obtained from the altimeters has been low-pass filtered before applying geostrophy in order to remove the white noise at short wavelength (cutoff wavelength of 40 km). In each case (model and observations), the velocities were high-pass filtered prior to compute the kinetic energy in order to retain only wavelengths below 200 km. Hereinafter, the resulting kinetic energy, representative of the energy below the mesoscale, will be referred as $KE_{\lambda<200km}$.

As expected from previous studies (e.g. Verron et al. 2015), along track $KE_{\lambda<200km}$ in the central GoM illustrates that the noise level is lower in Altika (Figure 3b) compared to Jason2 (Figure 3a). The levels of geostrophic $KE_{\lambda<200km}$ in the model compare well with Altika. Comparison between model based geostrophic $KE_{\lambda<200km}$ (Figure 3c,d) and $KE_{\lambda<200km}$ inferred directly from the model velocity normal to the track (Figures 3e,f) suggests that the geostrophic approximation allows to catch most of the spatial variability of the small scale features resolved by the model. High levels of $KE_{\lambda<200km}$ are observed in the Loop Current area, as expected by the ubiquitous presence of Loop Current Frontal Eddies (e.g. Jouanno et al. 2016a). The maximum of $KE_{\lambda<200km}$ in the northwestern GoM (near the shelf between 27°N-28°N and 94°W-88°W) described in Luo et al. (2016) using a model at 1-km resolution is also reproduced in our 1/36° simulation (Figure 3). It is worth mentioning that the altimetry data does not provide evidences of this maximum (Figure 3a,b). The scales involved (O (50) km) may be below the effective resolution of the altimeter and further observations may be required to confirm the presence of enhanced submesoscale activity near the northern GoM shelf.

Several regions with increased short-scale turbulence activity are identified from the temporal average of model $KE_{\lambda<200km}$ (computed using model surface velocity; Figure 4a). The seasonal variability of $KE_{\lambda<200km}$ present different regimes of variability. In the northwestern GoM, the GOLFO36 model shows a semi-annual cycle of $KE_{\lambda<200km}$ (Figure 4b). As mentioned in the introduction, such seasonal evolution has been described in Luo et al. (2016) with a higher resolution model (~1.6km). It consists of a dominant winter peak associated with the thermal front at the shelf break and a secondary late summer peak displaced ~100 km northward on the shelf and associated with the haline front of the Mississippi plume (not shown). In the open ocean, both in the western GoM (Figure 4c) and in the Loop Current area (Figure 4d), $KE_{\lambda<200km}$ follows an annual cycle with a peak of energy in winter that follows the mixed-layer depth seasonal cycle with one-month lag (not shown). Such behavior is in agreement with increased small scale turbulence in the deep winter mixed-layer (Sasaki et al. 2014, Callies et al. 2015). The 1-month lag can be interpreted as a consequence of meso/submesoscale energy build-up through available potential energy to eddy kinetic energy conversion by mixed-layer instabilities (which is directly proportional to mixed layer depth; Fox-Kemper et al 2008, Capet et al 2008). In the Loop Current area, the larger density gradients created during winter between the warm waters advected from the Caribbean Sea and the colder waters of the GoM, may also favor higher submesoscale activity in winter. In contrast with the above mentioned regions, the eastern shelf of the Campeche Bank shows a very weak semi-annual cycle, with more energy during winter and summer and a large standard deviation. This may be partly explained by the seasonal cycle of LCFEs dynamics along the Campeche Bank highlighted in Jouanno et al. (2016a) and associated with the seasonality of the cold surge events over the GoM.

4. **Vertical tracer exchanges**

With a horizontal grid spacing of ~3 km, the 1/36° simulation may only marginally be representative of the whole range of submesoscale dynamics in the GoM (Soufflet et al., 2016); nevertheless, we expect to be able to capture a significant fraction of its signature and effects. At lower resolution (1/12° and 1/4°), the kinetic energy at $\lambda < 200$km is well below the energy levels obtained in the 1/36°, at all scales and in all seasons (Figures 2b and 4). In this section, we will show that this has profound consequences on the vertical exchanges of the tracer.

Average surface tracer concentrations for the three model resolutions are shown after 30 days of integration starting from January 1 of each year from 1993 to 2012 (Figures 5j-l). We first focus on the winter period since this is the season with maximum short-scale turbulence activity (see Section 3.3; Figure 4) and as we will see below this is also the season with most sensitivity of mixed-layer depth and vertical tracer exchanges to model resolution. The strongest differences are in the northwestern part of the GoM, with larger tracer concentrations with decreasing resolution (Figures 5j-l), the difference being much larger between the 1/4° and 1/12° simulations than between the 1/12° and 1/36° simulations (Figure 5 and 6a). These differences in surface tracer concentrations appear linked with mixed-layer sensitivity to model resolution: the averaged mixed-layer depth in the northwestern part of the GoM is ~15 m larger in the lower resolution run compared to the higher resolution run.

This sensitivity of the mixed-layer depth is related to the presence of small-scale processes that actively contribute to the restratification of the upper ocean in the higher resolution simulations. As mentioned before, the largest impact of increasing resolution is seen in the northwestern part of the GoM, where the deepest mixed layers are found (see Figure 5).

The vertical tracer injection in the upper mixed layer seen after 30 days of model integration in the northwestern GoM (area between 24°N-28°N and 96°W-90°W) has a marked seasonal cycle (Figure 6), with more intense tracer exchange during winter when the mixed-layer is deep (O (100) m) and vanishing tracer exchange in summer when the mixed-layer is shallow (O (10) m). The sensitivity to model resolution is also greater in winter: increasing model resolution shallows the mixed-layer depth by about 30 meters and limits the tracer exchanges (Figure 6a). The monthly evolution of $KE_{\lambda<200km}$ and mixed-layer depth in the northwestern GoM is given in Figure 7a,b. From January to March, $KE_{\lambda<200km}$ shows an annual peak which follows with one-month lag the annual peak of mixed-layer depth. The vertical buoyancy flux averaged in the upper 200 meters ($<\overline{w'b'}>$ with w' and b' the vertical velocity and buoyancy anomalies with respect to horizontally averaged daily values over the area 24°N-28°N and 96°W-90°W, $<\cdot>$ the spatial averaging over this area, and $\overline{\cdot}$ the temporal averaging; Figure 7a) is also maximum from January to March. The eddy driven upward transport of buoyancy turns the upper layers more buoyant and acts to stratify the upper ocean (e.g., see Fox-Kemper et al. 2008). The vertical buoyancy flux is larger in the 1/36° simulation, so eddy-driven restratification is particularly active in this simulation, which reduces the mixed-layer depth and limits tracer exchanges.

It is important to note that the r.m.s. of the vertical velocity is much larger in the 1/36° simulation throughout the year (including in winter; Figure 7c) so we might have expected larger tracer exchanges between the mixed-layer and the subsurface in the high resolution run. The comparison of the different simulations contradicts this scenario and rather suggests that, to first order, the main effect of fine-scale dynamics on tracer distribution is through eddy-driven restratification.

In order to investigate how restratification acts during winter, GOLFO36 high-frequency outputs for winter 2011 are analyzed during a period of mixed-layer deepening (Figure 8). In January 2011, the GoM was under the influence of repeated northerly wind events (the Central American cold surges or "Nortes"; e.g. Schultz et al., 1998) that typically last 2 to 4 days and occur every 6-10 days. During these events, the air-sea fluxes act to cool down the ocean (Figure 8b), with a heat loss that reaches 800 W m^{-2} during night time (e.g. day 12 in Figure 8b). For each of these events, the mixed-layer deepened (Figure 8c) and the surface concentration of the tracer nutrient were increased (Figure 8d). This confirms that the vertical flux of tracer is strongly intermittent and, in the specific case of the GoM, it is primarily associated with intense atmospheric synoptic events.

The intermittent and chaotic shedding of Loop Current eddies travelling westward is expected to also modulate the evolution of mixed-layer and thermocline depths in the western GoM, so the direct comparison of the high frequency response in January 2011 in the different simulations may not be meaningful. To partially overcome this issue, we identified a total of 96 surface cooling events on the period 1993-2012, each reaching daily-averaged net air-sea heat flux larger than 400 W m^{-2}. The composite time evolution of mixed-layer depth and vertical buoyancy flux is shown in Figure 9. The averaged mixed-layer deepening (Figures 9a,b) in response to the cooling events (500 W m^{-2} in average; Figure 9d) is of order 15 meters. The mixed-layer anomalies (referenced to a mixed-layer depth averaged between days 3 to 5 prior to the peak of the wind event) illustrate that the differences observed between the simulations form in the two days following the wind event (Figure 9b). We link these differences with the eddy buoyancy flux which is particularly active during the few days encompassing the cooling event (Figure 9c). Eddy buoyancy fluxes are largest at the highest resolution as expected. This contributes to the reduction of the mixed layer deepening between the 1/12° and 1/36° solutions. $< \overline{w'b'} >$ values at the higher resolution are in line with previous estimates (Boccaletti et al. 2007, Brannigan et al. 2015, Capet et al. 2016) and are expected to further increase with increasing resolution.

5. Sensitivity under low-frequency wind-stress forcing

The high-frequency fluctuations of the wind stress during the passage of atmospheric fronts in the Gulf of Mexico force surface-intensified near-inertial waves (NIW; e.g. see Chen et al., 1996 or Jarosz et al. 2007 for observations in the Gulf of Mexico). A large fraction of the NIW energy is thought to dissipate close beneath the mixed-layer base, increasing vertical shear at the base of the mixed-layer and therefore causing entrainment (e.g., Price 1981; Cuypers et al. 2013; Jouanno et al, 2016b). In Section 4, we have shown that high-frequency winds shape the mixed-layer depth and contribute to the upward flux of tracer. One question that arises is how much of the mixed-layer deepening is simply due to mixed-layer convection in response to large surface cooling (due to air-sea heat fluxes) and how much is due to the mixing induced by the dissipation of the NIW at the mixed layer base. The presence of small scale eddy vorticity structures is known to accelerates the downward propagation of the wind-forced near-inertial waves (Danioux et al. 2011), so we expect some sensitivity of the NIW induced mixing to the model horizontal resolution.

This is investigated with the second set of simulations, forced with monthly wind stress, to remove inputs by the winds at the near-inertial scale (referred to as MONTHLY - see Section 2 for details). In these simulations there is no more wind driven input of near-inertial energy. As shown in Figure 10a,b, the winter mixed-layer depths are slightly reduced when removing the high-frequency winds (reduction of MLD of 5% at 1/4°, 13% at 1/12°, and 12% at 1/36°). The r.m.s. of the vertical velocity (Figures 10c,d) and the vertical flux of buoyancy (Figures 10e,f) in the upper 100 meters are also reduced at all the resolutions with larger differences found, again, for the 1/36° simulations. These results are consistent with those of Jouanno et al (2016b): for near-inertial processes to influence the ocean subsurface it is necessary to, at least, properly resolve the mesoscale activity, which in turn permits the downward propagation of near-inertial motions. Once mesoscale activity is resolved, near-inertial dissipation in the upper thermocline can have a significant impact. We note for example that there is more passive tracer depletion in the subsurface at 1/36° and high frequency forcings than at 1/12° with monthly winds. Likewise, we also note that the reduction of tracer fluxes exchanges between 1/4° and 1/36° resolution is significantly less with high frequency forcings. These comparisons illustrate the complexity of submesoscale impacts on vertical fluxes of properties, with antagonistic processes that respond differently to resolution increase and background conditions (e.g., during summer, removing the high frequency wind stress has almost no impact on the mixed-layer depth or on the upward flux of tracer, not shown).

6. Conclusions

This work investigates the role played by the meso- and submesoscale turbulence on the exchanges of passive tracers in the upper layers of the GoM using a hierarchy of regional simulations with horizontal resolution of 1/4°, 1/12° and 1/36° covering eddy present to submesoscale-rich regimes.

A careful evaluation of the model mesoscale activity in the GoM has been carried out using along-track data from recent altimeters. At scales larger than 100km, comparison of our higher resolution run with along-track altimetry shows that the model adequately represents the mesoscale field and spectral slope. But such exercise comes up against the high noise levels contained in altimetry products at scales below 50km, which did not allow us to evaluate the realism of the submesoscale field reproduced by the higher resolution simulation.

In agreement with the present understanding of submesoscale dynamics, vertical velocity variance in the northwestern GoM increases strongly for increasing horizontal resolution (e.g. Zhong and Braco, 2013). On the other hand, contrary to many previous studies demonstrating that submesoscales enhance surface-subsurface exchanges (through frontogenetic circulations; Klein and Lapeyre 2009, Lévy et al. 2001, Spall and Richards 2000, Mahadevan and Archer 2000) we find that explicitly resolving submesoscale processes may actually limit the exchanges between the surface and the subsurface. Precisely, as shown in our study, submesoscale impacts vertical exchanges of properties in several antagonistic ways. At dx=1km, fluxes of buoyancy are enhanced in the upper ocean (compared to lower resolution simulations), which yields a stronger upper ocean stratification (Couvelard et al, 2015), hence a reduction of vertical fluxes of passive or biogeochemical tracers. On the other hand, enhanced resolution favors the penetration of near-inertial motions below the mixed layer which tends to strengthen mixing and vertical exchanges. The outcome of these two competing effects depends on the particular distribution of the considered tracer, on the amount of near-inertial energy deposited in the mixed layer, on the Brunt-Vaisala profile, etc. With numerical resolution around a few kilometers our passive tracer experiments suggest that both effects are of comparable magnitude.

This seems to go against the current view that submesoscales would increase nutrient fluxes into the euphotic layer (Lévy et al. 2001, Spall and Richards 2000, Mahadevan and Archer 2000). However, interpretation of our results in terms of real biogeochemical tracers (typically nutrients) should be done with caution. In an equilibrated simulation with explicit representation of biogeochemical sources and sinks the sensitivity to resolution may be felt somewhat differently than in our simulations. Over time, the distribution of nutrients may indeed adjust to stratification, and thus, at high resolution, develop larger values in the depth range where fluxes are reduced compared to lower resolution. On the other hand, we expect the winter-time vertical distribution of nutrients in the GoM to be also controlled by external processes, *e.g.*, subsurface replenishment through lateral transport by the mean flow and mesoscale turbulence in summer and fall. In such conditions, our numerical protocol where a unique initial tracer distribution is prescribed with no dependence to resolution might thus provide useful insight into submesoscale impact on nutrient fluxes. Analyses of coupled physics-biogeochemistry simulations will be needed to confirm that GoM winter submesoscales are detrimental to the injection of subsurface nutrients.

Acknowledgements: This study was supported by CIGOM. We acknowledge the provision of supercomputing facilities by CICESE and GENCI project GEN7298. Altimetry data were produced by Salto/Duacs and distributed by AVISO, with support from CNES. We are grateful to Rachid Benshila and Jerome Chanut for their help with the ocean model. The along-track altimetry data were pre-processed with the Python package py-altimetry-0.3.2.

References

Ascani, F., K.J. Richards, E. Firing, S. Grant, K.S. Johnson, Y. Jia, R. Lukas and D.M. Karl (2013). Physical and biological controls of nitrate concentrations in the upper subtropical North Pacific Ocean. Deep Sea Research Part II: Topical Studies in Oceanography, 93, 119-134.

Boccaletti, G., R. Ferrari, and B. Fox-Kemper (2007). Mixed layer instabilities and restratification. J. Phys. Oceanogr., 2228–2250.

Bracco, A., J. Choi, K. Joshi, H. Luo, and J.C. McWilliams (2016). Submesoscale currents in the Northern Gulf of Mexico: deep phenomena and dispersion over the continental slope. Ocean Modelling, 101, 43-58.

Brannigan, L., D. P. Marshall, A. Naveira-Garabato, and A. G. Nurser (2015). The seasonal cycle of submesoscale flows. Ocean Modelling, 92, 69-84.

Callies, J., R. Ferrari, J.M. Klymak, and J. Gula (2015). Seasonality in submesoscale turbulence. Nature communications, 6.

Capet, X., J.C. McWilliams, M.J. Molemaker, and A.F. Shchepetkin (2008). Mesoscale to sub-mesoscale transition in the California current system. Part III: Energy balance and flux. J. Phys. Oceanogr. 38, 2256–2269.

Capet, X., G. Roullet, P. Klein, and G. Maze (2016). Intensification of upper ocean submesoscale turbulence through Charney baroclinic instability. J. Phys. Oceanog., 46, 3365–3384, doi: 10.1175/JPO-D-16-0050.1.

Chen, C., R. O. Reid, and W. Nowlin, (1996). Near-inertial oscillations over the Texas-Louisiana shelf. J. Geophys. Res., 101(C2): 3509–3524.

Couvelard, X., F. Dumas, V. Garnier, A. L. Ponte, C. Talandier, and A. M. Treguier (2015). Mixed Layer formation and restratification in presence of mesoscale and submesoscale turbulence. Ocean Modelling, 96, 243-253.

Dai, A. and K. E. Trenberth (2002). Estimates of freshwater discharge from continents: Latitudinal and seasonal variations. J. Hydrometeorol., 3, 660-687.

Danioux, E., P. Klein, M. W. Hecht, N. Komori, G. Roullet, and S. Le Gentil (2011). Emergence of wind-driven near-inertial waves in the deep ocean triggered by small-scale eddy vorticity structures. Journal of Physical Oceanography, 41(7), 1297-1307.

Dufau, C., M. Orsztynowicz, G. Dibarboure, R. Morrow, and P. Y. Le Traon (2016). Mesoscale resolution capability of altimetry: Present and future. Journal of Geophysical Research: Oceans, 121(7), 4910-4927.

Dussin, R., B. Barnier and L. Brodeau (2016). The making of Drakkar forcing set DFS5. DRAKKAR/MyOcean Report 01-04-16, LGGE, Grenoble, France.

Fox-Kemper, B., R. Ferrari, and R. Hallberg (2008). Parameterization of mixed layer eddies. Part I: Theory and diagnosis. Journal of Physical Oceanography, 38(6), 1145-1165.

Hetland, R. D. (2017). Suppression of baroclinic instabilities in buoyancy driven flow over sloping bathymetry. Journal of Physical Oceanography, doi:10.1175/JPO-D-15-0240.1.

Jarosz, E., Z. Hallock, and W. Teague, (2007). Near-inertial currents in the DeSoto Canyon Region. Continental Shelf Research, 27, 2407-2426.

Jouanno, J., X. Capet, G. Madec, G. Roullet, and P. Klein (2016b). Dissipation of the energy imparted by mid-latitude storms in the Southern Ocean. Ocean Sci. 12, 743-769, doi:10.5194/os-12-743-2016.

Jouanno, J., J. Ochoa, E. Pallàs-Sanz, J. Sheinbaum, F. Andrade, J. Candela, J.M. Molines (2016a). Loop Current Frontal Eddies: formation along the Campeche Bank and impact of coastally trapped waves. Journal of Physical Oceanography, 46(11), 3339-3363.

Klein, P. and G. Lapeyre (2009). The oceanic vertical pump induced by mesoscale and submesoscale turbulence. Annual Review of Marine Science, 1, 351-375.

Large, W. G. and S. Yeager (2009). The global climatology of an interannually varying air-sea ux data set. Climate Dynamics, 33, 341-364, doi:10.1007/s00382-008-0441-3.

Leclair, M. and G. Madec (2009). A conservative leapfrog time stepping method. Ocean Modelling, 30, 88-94.

Le Hénaff, M., V. H. Kourafalou, R. Dussurget, and R. Lumpkin (2014). Cyclonic activity in the eastern Gulf of Mexico: Characterization from along-track altimetry and in situ drifter trajectories. Progress in Oceanography, 120, 120-138.

Lévy, M., D. Iovino, L. Resplandy, P. Klein, G. Madec, A. M. Tréguier, S. Masson and K. Takahashi (2012). Large-scale impacts of submesoscale dynamics on phytoplankton: Local and remote effects. Ocean Modelling, 43, 77-93.

Lévy, M., P. Klein, A. M. Tréguier, D. Iovino, G. Madec, S. Masson, and K. Takahashi (2010). Modifications of gyre circulation by sub-mesoscale physics. Ocean Modelling, 34(1), 1-15.

Lévy M, P. Klein, and A.M. Treguier (2001). Impacts of sub-mesoscale physics on production and subduction of phytoplankton in an oligotrophic regime. J. Mar. Res. 59, 535–65.

Luo, H., A. Bracco, Y. Cardona, and J.C. McWilliams (2016). Submesoscale circulation in the northern Gulf of Mexico: surface processes and the impact of the freshwater river input. Ocean Modelling, 101, 68-82.

Madec, G. and the NEMO team (2016). "NEMO ocean engine". Note du Pôle de modélisation, Institut Pierre-Simon Laplace (IPSL), Paris, France, No 27 ISSN No 1288-1619.

Mahadevan, A. and D. Archer (2000). Modeling the impact of fronts and mesoscale circulation on the nutrient supply and biogeochemistry of the upper ocean. J. Geophys. Res. Oceans 105:1209–25.

McWilliams, J. C. (2016). Submesoscale currents in the ocean. In Proc. R. Soc. A, Vol. 472, No. 2189, p. 20160117.

Reffray G., R. Bourdalle-Badie and C. Calone (2015). Modelling turbulent vertical mixing sensitivity using a 1-D version of NEMO. Geosci. Model Dev., 8, 69–86, doi:10.5194/gmd-8-69-2015.

Rosso, I., A. M. Hogg, P. G. Strutton, A. E. Kiss, R. Matear, A. Klocker, and E. van Sebille (2014). Vertical transport in the ocean due to sub-mesoscale structures: Impacts in the Kerguelen region. Ocean Modelling, 80, 10-23.

Sasaki, H., P. Klein, B. Qiu, and Y. Sasai (2014). Impact of oceanic-scale interactions on the seasonal modulation of ocean dynamics by the atmosphere. Nat. Commun., 5, 5636, doi:10.1038/ncomms6636.

Schultz, D. M., W. E. Bracken, and L. F. Bosart (1998). Planetary- and synoptic-scale signatures sssociated with central american cold surges. Mon. Wea. Rev., 126, 5–27.

Shriver, J. F., B. K. Arbic, J. G. Richman, R. D. Ray, E. J. Metzger, A. J. Wallcraft, and P. G. Timko (2012). An evaluation of the barotropic and internal tides in a high-resolution global ocean circulation model. J. Geophys. Res., 117, C10024, doi:10.1029/2012JC008170.

Soufflet, Y., P. Marchesiello, F. Lemarié, J. Jouanno, X. Capet, L. Debreu, and R. Benshila (2016). On effective resolution in ocean models. Ocean Modelling, 98, 36-50.

Spall S.A. and K.J. Richards (2000). A numerical model of mesoscale frontal instabilities and plankton dynamics—I. Model formulation and initial experiments. Deep-Sea Res. I 47:1261–301.

Umlauf, L. and H. Burchard (2003). A generic length-scale equation for geophysical turbulence models. Journal of Marine Research, 61 (31), 235–265.

Verron, J., P. Sengenes, J. Lambin, J. Noubel, N. Steunou, A. Guillot, N. Picot, S. Coutin-Faye, R. Sharma, R. M. Gairola, D. V. A. R. Murthy, J. G. Richman, D. Griffin, A. Pascual, F. Rémy, and P. K. Gupta (2015). The SARAL/AltiKa altimetry satellite mission. Marine Geodesy, 38(sup1), 2-21.

Xu, Y. and L. L. Fu (2012). The effects of altimeter instrument noise on the estimation of the wavenumber spectrum of sea surface height. Journal of Physical Oceanography, 42(12), 2229-2233

Zhong, Y. and A. Bracco (2013). Submesoscale impacts on horizontal and vertical transport in the Gulf of Mexico. Journal of Geophysical Research: Oceans, 118(10), 5651-5668.

Name	Horizontal resolution	Δx, Δy	Δt	Laplacian diffusivity coefficient
GOLFO36	1/36°	~2.8 km	150s	45 m^2 s^{-1}
GOLFO12	1/12°	~8.4 km	600s	135 m^2 s^{-1}
GOLFO04	¼ °	~25.2 km	1800s	405 m^2 s^{-1}

Table 1: Description of the three reference simulations used in this study.

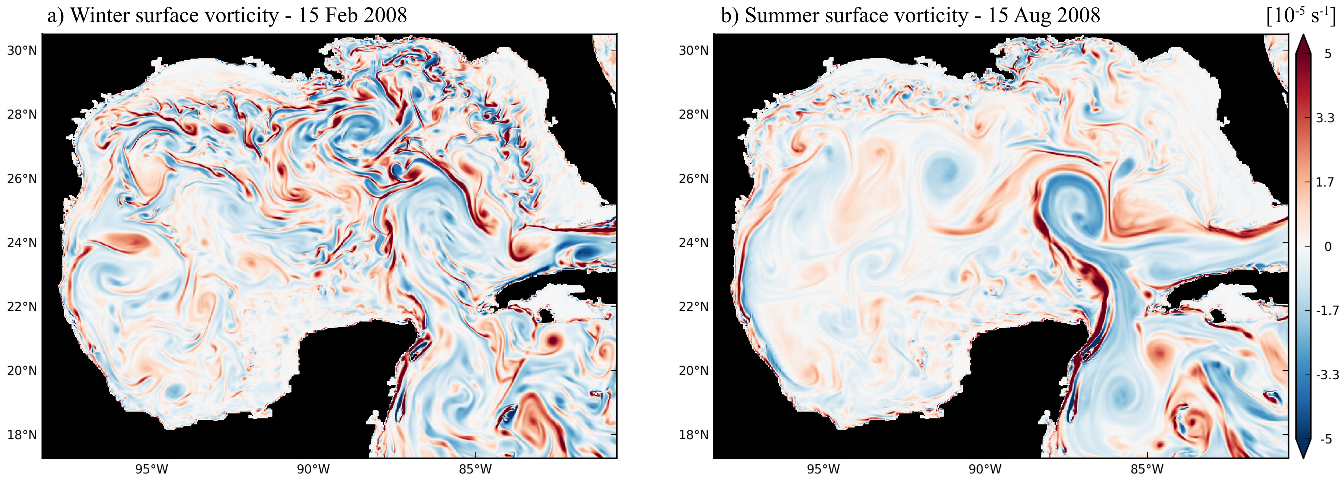

Figure 1. Snapshots of surface vorticity simulated by GOLFO36 at days 15 February 2008 (a) and 15 August 2008 (b). We identify mesoscale structures (the Loop Current, anticyclones close that have been shed by the Loop Current), and submesoscale structures including filaments.

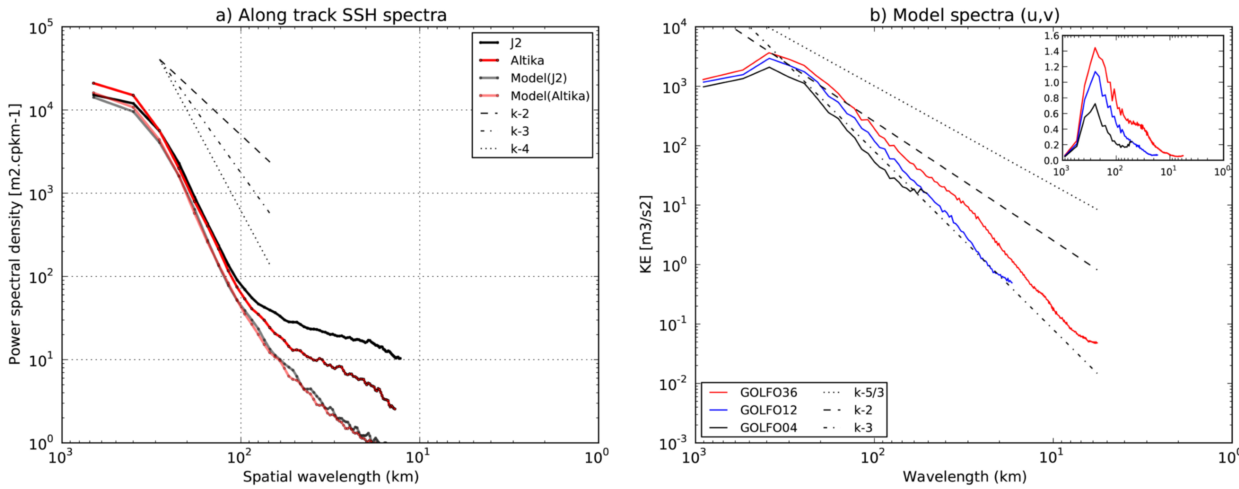

Figure 2. a) Along track wavenumber spectra from altimetry SSH (Jason2 in black, Altika in red) and GOLFO36 model SSH (along Jason2 tracks in light black and along Altika tracks in light red). A multitaper method with taper of 600km has been used. The model data have been interpolated along the satellite tracks. b) KE spectra for the horizontal velocity $\mathbf{u}_h$ at 10-m depth for the three simulations at 1/36 °, 1/12° and ¼° plotted as a function of horizontal wavenumber magnitude, $k = |\mathbf{k}_h|$; so the 2D spectrum is azimuthally integrated in k shells following the method described in Capet al. (2008c). The corresponding variance conserving spectra are shown in the inset (units 10^{-6} m s^{-2}). Daily averages model data from 98W to 82W and 18N to 30N and from 2008 to 2012 have been used and the spectra have been temporally averaged. The k^{-2}, k^{-3} and $k^{-5/3}$ spectral slope are also shown.

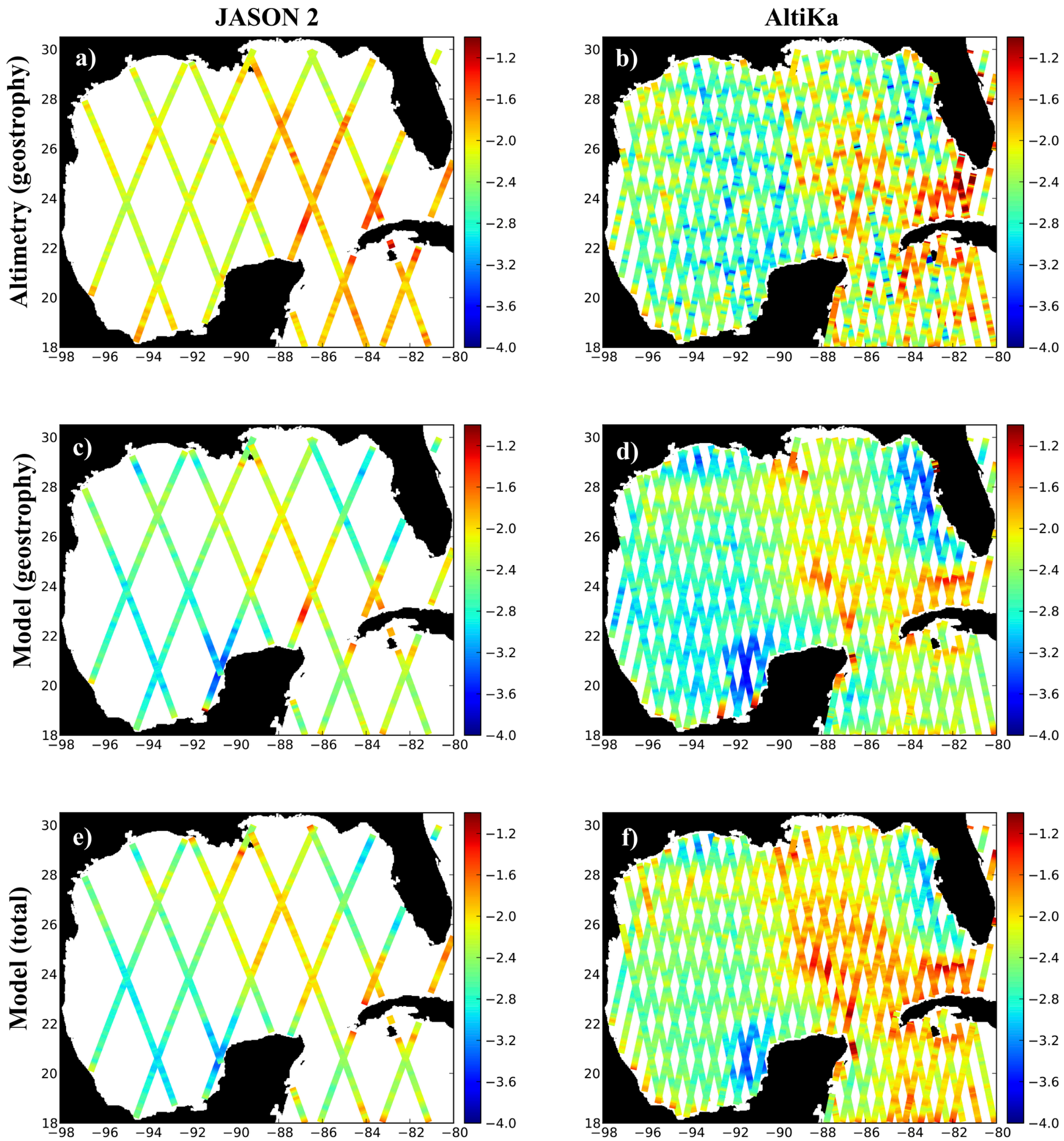

Figure 3. KE [log10 m^2s^{-2}] in the 40-200km band obtained from along track altimetry SSH (top), GOLFO36 model SSH (middle), and surface velocity (bottom). The altimetry SSH has been filtered with a 40km low pass filter before applying geostrophy. The left column is for Jason2 and the right column is for AltiKa data.

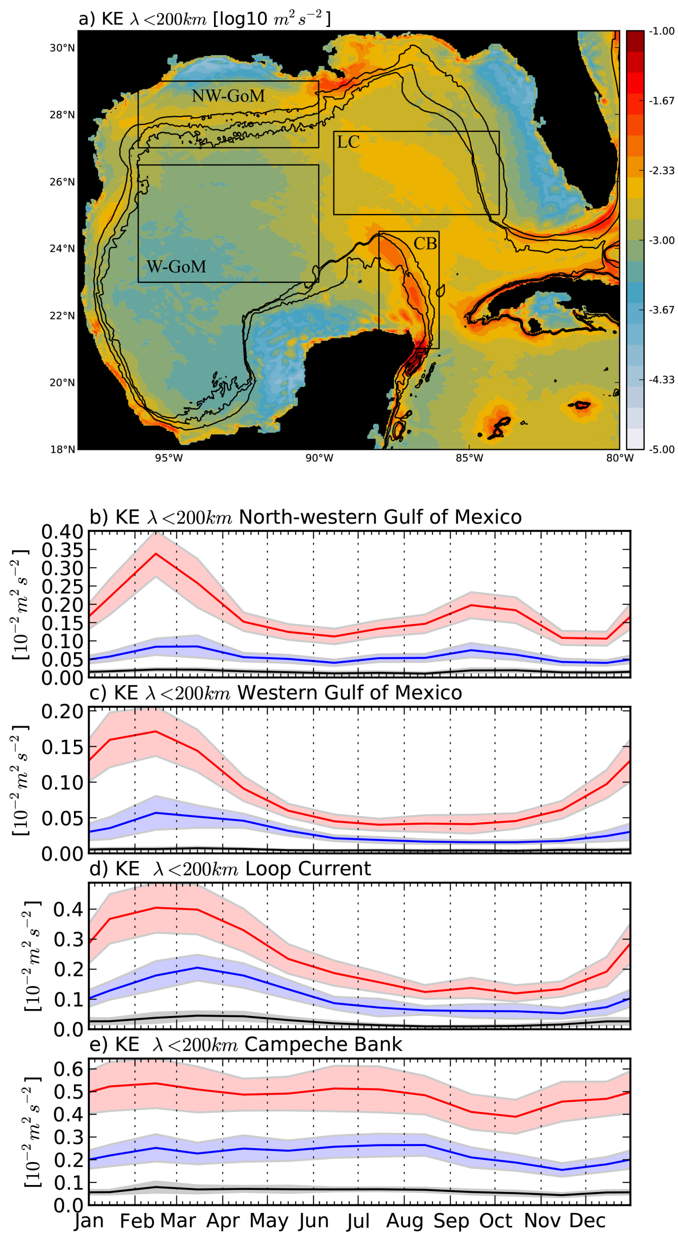

Figure 4. KE ($m^2 s^{-2}$) computed from high-pass filtered (λ < 200km) surface velocity anomalies : mean distribution in GOLFO36 (a) and seasonal cycle of $KE_{\lambda<200km}$ spatially averaged over four different regions (b-e), for the three simulations (GOLFO36 in red, GOLFO12 in blue and GOLFO04 in black). Daily data from 2003 to 2012 have been used and the enveloppes indicate the monthly s.t.d. of the daily values of KE.

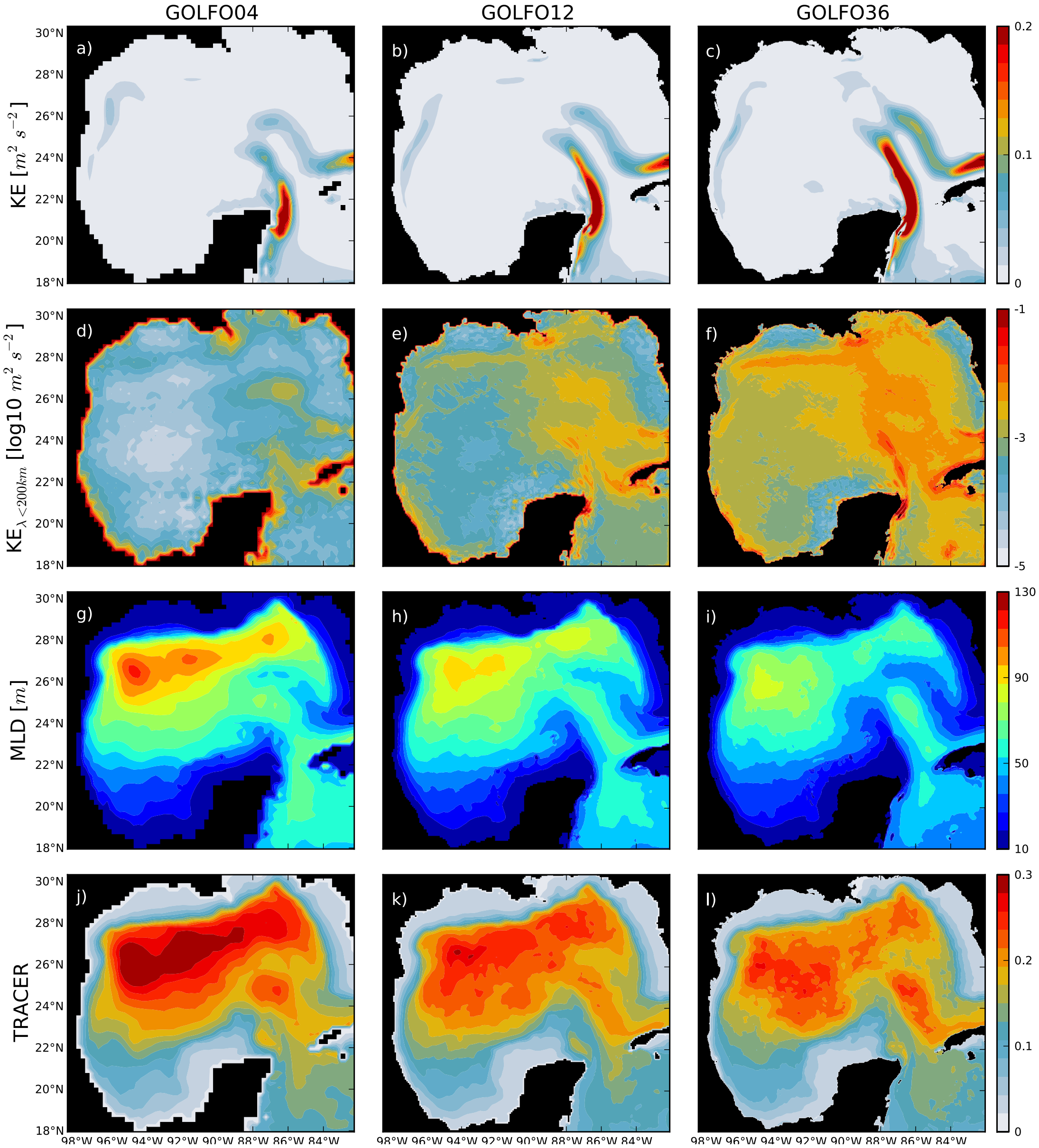

Figure 5. Winter (a) mean surface kinetic energy ($m^2\ s^{-2}$), (b) mean $KE_{\lambda<200km}$ (log10 $m^2\ s^{-2}$) computed from high-pass filtered (λ < 200km) surface velocity, (c) mean mixed-layer depth (MLD; unit m), and (d) 5-day mean averaged surface distribution of passive tracers "NUTRIENT" after 30 days of transport in the 1/4° (left), 1/12° (center) and 1/36° (right) simulations. The MLD criterion used in this study corresponds to the depth at which density is 0.03 kg m^{-3} larger than the density at 10 m depth. Data from 1 January to 14 March of each year from 1993 to 2012 are considered and the tracers were initialized at five different dates (regularly spaced; see text) for each year from 1993 to 2012.

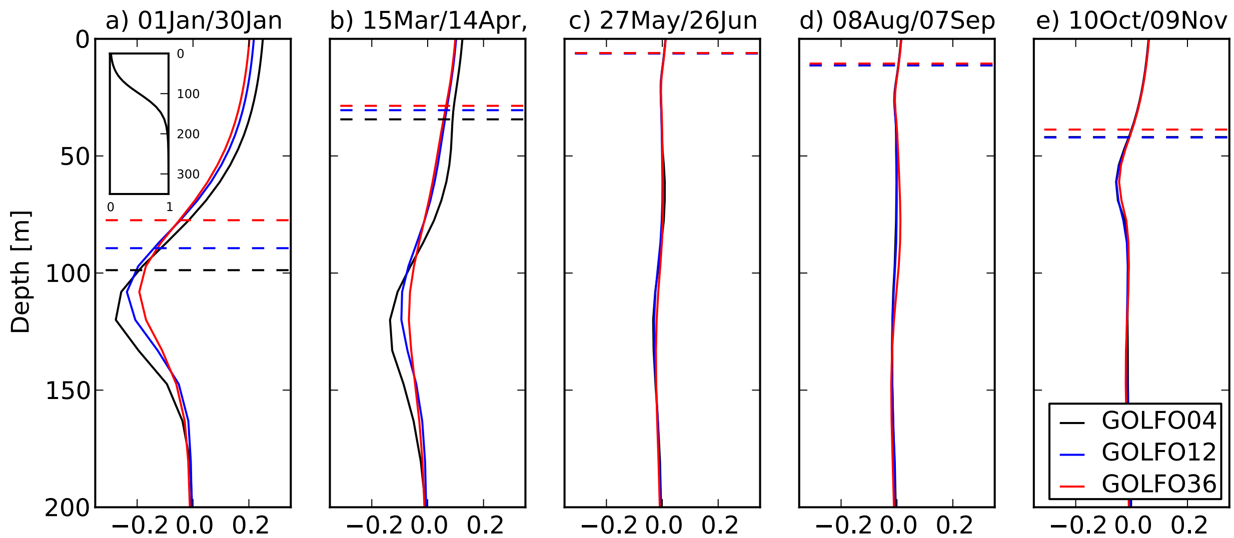

Figure 6. Results of on-line transport experiments of the passive tracer "NUTRIENT" performed for the 1/4°, 1/12° and 1/36° simulations and averaged over the northwestern GoM (96°W-90°W, 24°N-28°N). The tracer was initialized at the five same dates of each year (a-e) from 1993 to 2012. The initial state is uniform in the horizontal, with a vertical gradient on the vertical, increasing from 0 at the surface to 1 at 200 m and below. Vertical profiles of the tracer anomaly (i.e. the difference between the final profile and the initial profile) are shown after 30 days of transport. The horizontal dashed lines indicate the averaged mixed-layer depth for each 30-day period.

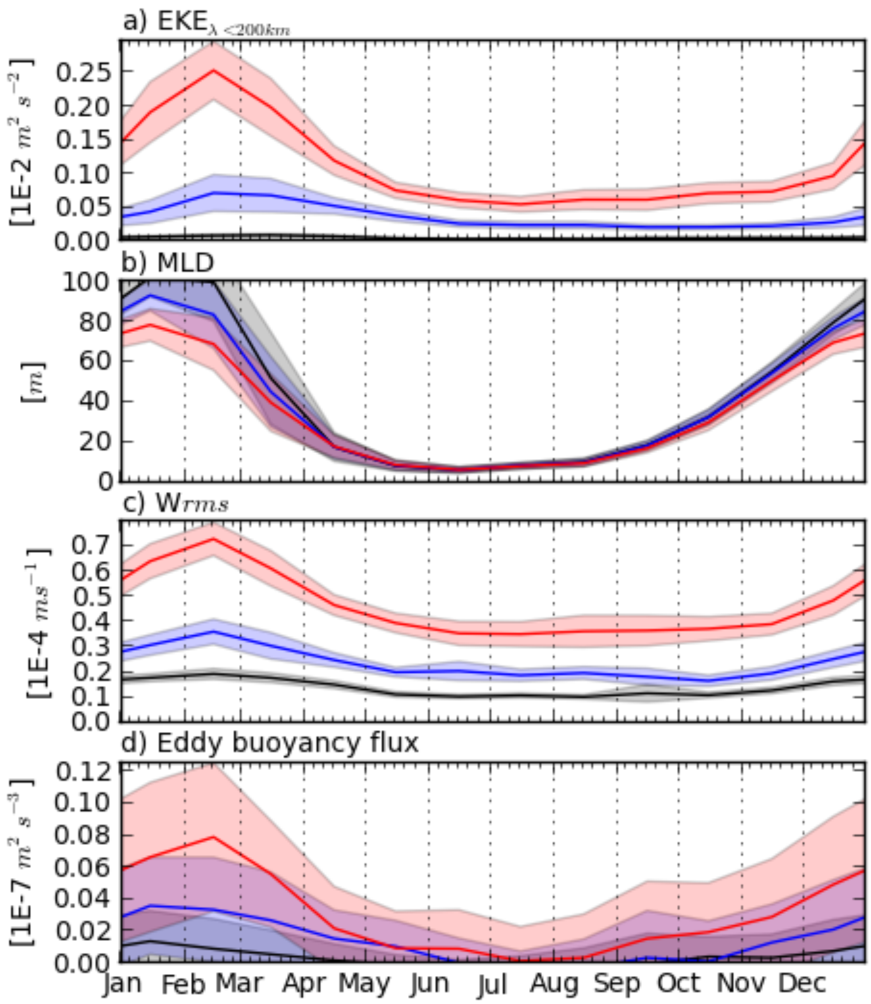

Figure 7. Seasonal cycle of (a) surface EKE$_{\lambda<200km}$ (N m^{-2}) computed from high pass filtered (λ < 200km) horizontal velocity anomalies, (b) mixed-layer depth (m), (c) the r.m.s. of the vertical velocity averaged in the upper 200 meters (m s^{-1}) and (d) the eddy buoyancy flux $< \overline{w'b'} >$ averaged in the upper 200 meters (m^2 s^{-3}). The seasonal cycles are built using daily data of the three different simulations (GOLFO36 in red, GOLFO12 in blue and GOLFO04 in black) from 1993 to 2012, and were averaged in the northwestern GoM (96°W-90°W, 24°N-28°N). The monthly standard deviation is displayed in light colors.

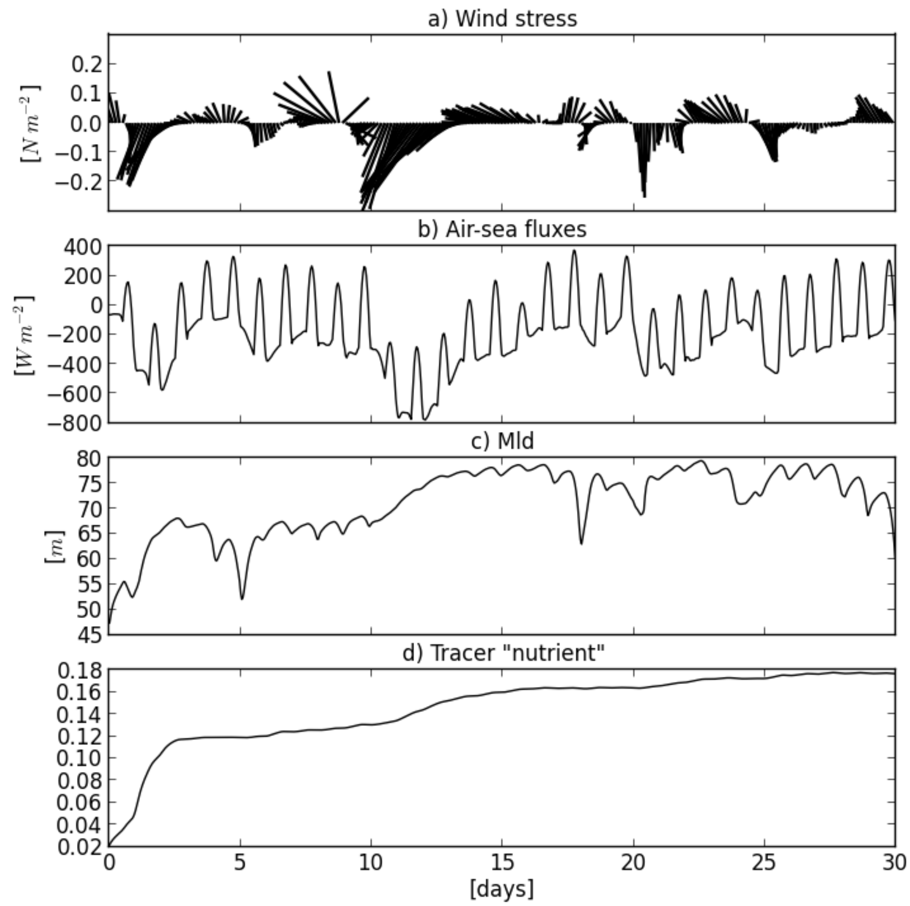

489 **Figure 8.** Hourly time series of 1/36° model fields averaged in the northwestern GoM (96°W-
490 90°W, 24°N-28°N) from days 1 to 31 January 2011 : (a) wind stress (N m^{-2}), (b) net air-sea
491 fluxes (W m^{-2}), (c) mixed-layer depth (m) and (d) surface concentration of tracer "Nutrient"
492 initialized at day 0 in GOLFO36.

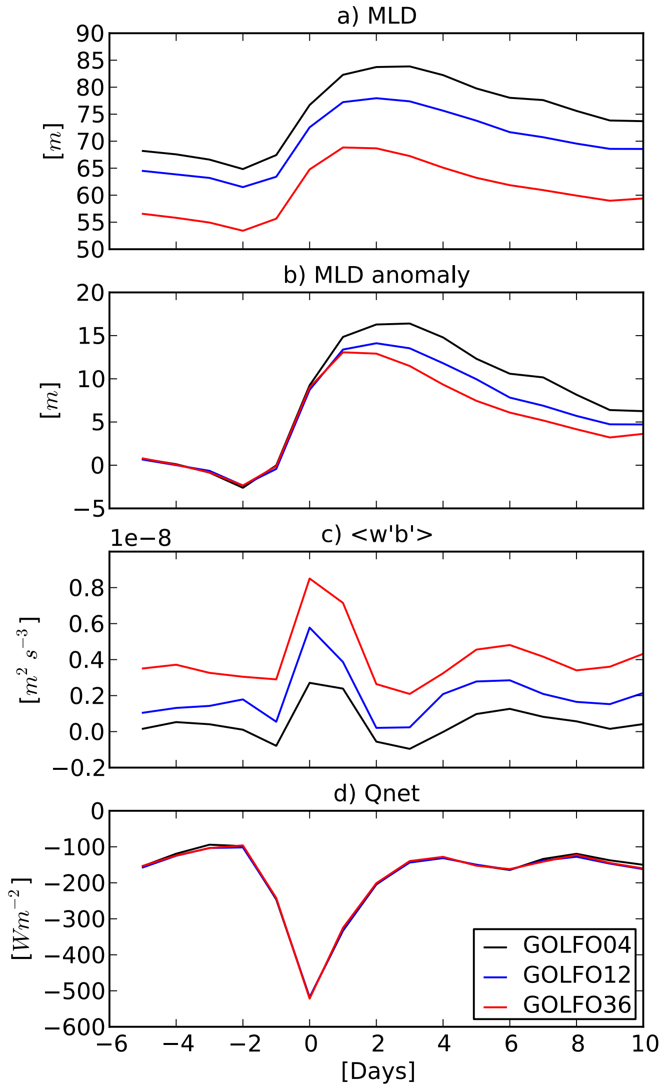

Figure 9. Lagged composites based on 96 events identified with upward daily averaged net –air-sea heat flux larger than 400 W m^{-2}, obtained for the reference set of simulations: a) mixed-layer depth (m), b) mixed-layer depth anomaly (m) referenced to the mixed-layer depth averaged between lags -5 to -3 days, c) vertical buoyancy flux $<\overline{w'b'}>$ averaged between 0 and 200 meters (m^2 s^{-3}) and d) net air-sea heat flux (W m^{-2}; negative means upward). Daily data from 1994 to 2012 have been used.

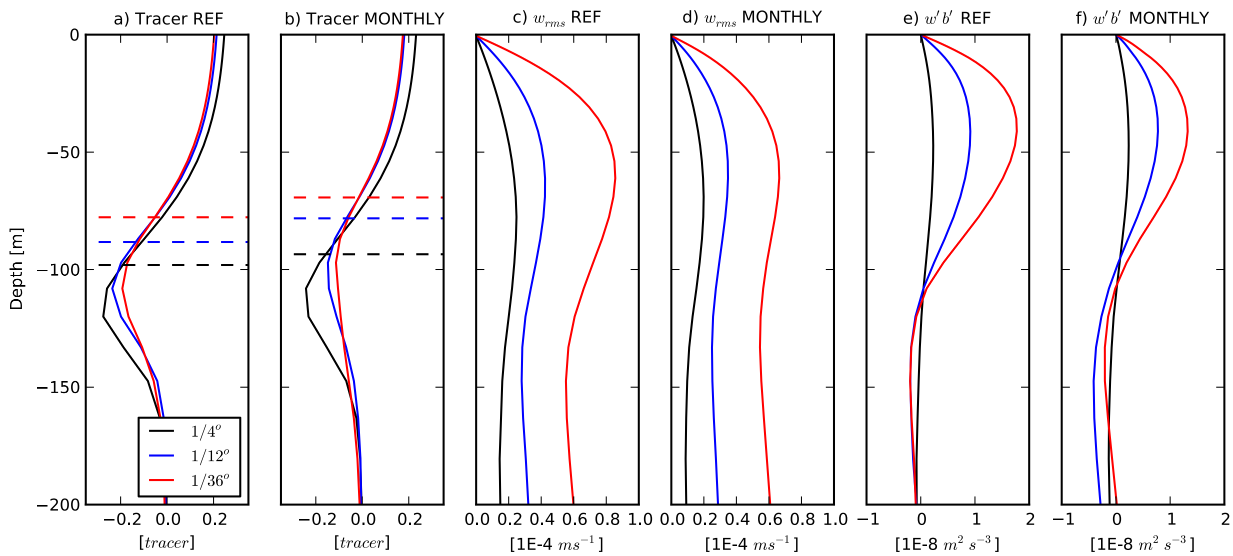

Figure 10. Comparison between the reference set of simulations forced with 3-hours wind stress (REF) and the simulations forced with monthly wind stress (MONTHLY) during winter: a,b) passive tracer anomaly after 30 days of transport during the winter period (as in Figure 6a), c,d) r.m.s. of the vertical velocity (m s^{-1}) and e,f) vertical buoyancy flux $< \overline{w'b'} >$ (m^2 s^{-3}). All the diagnostics have been made using data from January 1 to March 14 for year from 1994 to 2012 and were averaged in the northwestern GoM (96°W-90°W, 24°N-28°N).